Available online at www.sciencedirect.com
ScienceDirect
Journal of Power Sources 171 (2007) 663–669
JOURNAL OF POWER SOURCES
www.elsevier.com/locate/jpowsour

An efficient ceramic-based anode for solid oxide fuel cells

Qingxi Fu [a,*], Frank Tietz [a], Doris Sebold [a], Shanwen Tao [b], John T.S. Irvine [b]

[a] *Institute for Energy Research (IEF-1), Forschungszentrum Jülich GmbH, 52425 Jülich, Germany*
[b] *School of Chemistry, University of St. Andrews, KY16 9ST Scotland, United Kingdom*

Received 1 October 2006; received in revised form 20 June 2007; accepted 24 June 2007
Available online 29 June 2007

Abstract

A new ceramic-based multi-component material, containing one electronic conductor (Y-substituted $SrTiO_3$, SYT), one ionic conductor (YSZ) and a small amount (∼5 vol.%) of Ni catalyst, was investigated as an alternative anode material for solid oxide fuel cells (SOFCs). The ceramic framework SYT/YSZ shows good dimensional stability upon redox cycling and has an electrical conductivity of ∼10 S cm^{-1} under typical anode conditions. Owing to the substantial electrocatalytic activity of the fine and well-dispersed Ni particles on the surface of the ceramic framework, the electrode polarization resistance of 5 vol.% Ni-impregnated SYT/YSZ anode reached 0.21 Ω cm^2 at 800 °C in wet Ar/5%H_2. Based on these results, a redox-stable anode-supported planar SOFC is expected using this anode material, thus offering great advantages over the current generation of Ni/YSZ-based SOFCs.

Keywords: Ceramic; Electrochemical property; Anode material; Redox; Solid oxide fuel cells

1. Introduction

An anode-supported planar design is favored by many solid oxide fuel cell (SOFC) developers since it allows the operating temperature to be reduced to the range of 700–800 °C whilst retaining the same power density as electrolyte-supported cells at 950 °C [1]. This will in turn increase the cell lifetime and allow costs to be reduced by using less expensive interconnect materials. In the state-of-the-art anode material, a Ni/YSZ cermet, the nickel does not only serve as a good catalyst for fuel oxidation, but also as a good current collector. To ensure sufficient current collection, the nickel content is usually over 35 vol.% to form a percolation path for electron transport. However, the nickel component of the anode may be reoxidized in a commercial SOFC system due to situations such as seal leakage, fuel supply failure or system shutdown or possibly even very high fuel utilization. Thus cyclic reduction and oxidation (redox cycling) of the anode is likely to occur during commercial SOFC operation. The reduction and oxidation of Ni is accompanied by large volume changes, which may cause fracture either of the anode itself or of its adjacent component, the thin electrolyte layer [2–5]. The use of a reducing purge gas [6] can prevent the anode from being oxidized, but this will also increase system complexity and cost. Therefore this approach is not attractive, especially not for small-scale residential CHP (combined heat and power) systems. Another possible solution is to optimize the microstructure and/or Ni content in the present Ni/YSZ anode material. However, this can only alleviate the problem to a very limited extent as long as Ni has to take on the role of electronic conduction in the electrode [7,8]. Therefore, it is desirable to develop alternative anode materials that are dimensionally stable upon redox cycling while maintaining good electrochemical performance as Ni/YSZ anodes.

Ceramic oxides with significant electronic conductivity are considered as good candidate materials since they have generally good dimensional stability upon redox cycling. Therefore ceramic oxides with various crystalline structures have been investigated as alternative anode materials [9–15]. However, few of them exhibit both good electrochemical performance and high electronic conductivity. Some oxides, e.g. $Nb_{0.67}Ti_{0.33}O_{2\pm\delta}$ [9]

* Corresponding author. Tel.: +49 2461 615007; fax: +49 2461 612455.
E-mail address: qxfu@hotmail.com (Q. Fu).

0378-7753/$ – see front matter © 2007 Elsevier B.V. All rights reserved.
doi:10.1016/j.jpowsour.2007.06.159

and La-substituted $SrTiO_3$ [10,11], are very good electronic conductors (>20 S cm^{-1}), but exhibit very poor electrocatalytic activity for fuel oxidation, possibly due to the lack of significant ionic conductivity in these materials [9]. Some oxides, e.g. doped ceria [12,13] and $(La_{0.75}Sr_{0.25})_{1-x}Cr_{0.5}Mn_{0.5}O_{3-\delta}$ ($0 \leq x \leq 0.1$) (LSCM) materials [14,15], show fairly good electrocatalytic activity at least for the oxidation of hydrogen, but their electronic conductivity is only in the order of 1 S cm^{-1} under operating conditions, which is two orders of magnitude lower than that of the state-of-the-art Ni/YSZ material. In fact, even for these materials, their electrocatalytic activity is still lower than the Ni/YSZ material and needs to be further improved, especially with respect to the oxidation of methane.

To improve the electrocatalytic activity of ceria-based anodes, Primdahl and Liu [16] and Uchida et al. [17] incorporated a small amount (<10 vol.%) of Ni catalyst into the ceramic framework and found it very effective. Liu et al. [18] added another ceramic component, forming a three-component material, $La_{0.8}Sr_{0.2}Cr_{0.8}Mn_{0.2}O_{3-\delta}$–$Ce_{0.9}Gd_{0.1}O_{1.95}$–Ni, in which $La_{0.8}Sr_{0.2}Cr_{0.8}Mn_{0.2}O_{3-\delta}$ acted as an electronic conductor and $Ce_{0.9}Gd_{0.1}O_{1.95}$ as an ionic conductor while 4 wt% Ni is necessary to obtain good catalytic activity for hydrocarbon oxidation. However, this composite anode material has an electrical conductivity of well below 1 S cm^{-1} [18] under anode conditions due to the insufficient electrical conductivity of $La_{0.8}Sr_{0.2}Cr_{0.8}Mn_{0.2}O_{3-\delta}$ in reducing atmospheres. The electronic conductivity of the p-type conductor $La_{0.8}Sr_{0.2}Cr_{0.8}Mn_{0.2}O_{3-\delta}$ is ~8 S cm^{-1} in air [18], and it should be appreciably lower (roughly by one order of magnitude) in reducing atmosphere like (La,Sr)CrO_3 [19]. As a reference, the material $La_{0.75}Sr_{0.25}Cr_{0.5}Mn_{0.5}O_{3-\delta}$ has an electrical conductivity of 38 S cm^{-1} in air, but only 1.5 S cm^{-1} in Ar/5% H_2 at 900 °C [15]. The relatively low electrical conductivity of an anode material would necessitate the addition of an appropriate current collector, and may also hinder the electrochemical reaction kinetics.

In the present work, we adopted a very good electronic conductor, yttrium-substituted $SrTiO_3$ (SYT), as one component of the anode in order to improve its electronic conductivity and also to facilitate the electrochemical reactions. Compared with LSCM, SYT shows much higher electrical conductivity under anode conditions. With a nominal yttrium content of 7–10 at.%, the electrical conductivity of SYT can reach 20–100 S cm^{-1} at 800 °C [20,21]. In addition, SYT shows very small chemical expansion upon redox cycling (see below). YSZ was then combined with SYT to supply the ionic conduction path, and additionally a small amount of Ni catalyst was incorporated into the two-phase ceramic network to enhance the catalytic activity. The composition and function of each component in this multi-component ceramic-based anode is summarized in Table 1.

2. Experimental

2.1. Sample preparation

Dense electrolyte (8YSZ) substrate pellets (Ø 20 mm and ~2 mm thick) were prepared by uniaxial pressing of commercial YSZ powder (Tosoh TZ-8Y) and sintering in air at 1500 °C for 10 h. SYT ($Sr_{0.93}Y_{0.07}TiO_3$) powder was prepared by the Pechini method [22] and was reduced in Ar/4%H_2 at 1300 °C for 12 h before use.

Two methods were used to incorporate Ni into the electrodes. In the first method, the SYT/YSZ paste was applied onto one side of the YSZ substrate by screen printing. The paste was prepared with the aid of a three-roll mill using 6% ethyl cellulose in terpineol as a binder. After de-binding in air at 700 °C, the electrode was then sintered in Ar/4% H_2 at 1200–1300 °C for 3 h to form a porous ceramic framework with ~40% porosity. The sintering was performed in reducing atmospheres in order to retain the high electronic conductivity of the pre-reduced SYT phase. Subsequently, the pores were impregnated with nickel nitrate ($Ni(NO_3)_2{\cdot}6H_2O$, Fluka) solution followed by thermal decomposition at 800 °C to form nickel oxide. The process of impregnation and decomposition was repeated until the desired level of Ni loading was obtained. In the present study, three and six cycles was required to incorporate 5 and 10 vol.% of Ni into the porous electrodes, respectively.

In the second method, NiO powder with an average particle size of 10–20 nm (Sigma–Aldrich) was directly mixed with SYT/YSZ by ball milling and then applied onto the YSZ substrates by screen printing, followed by sintering in Ar at 1200–1300 °C for 3 h. Here Ar instead of Ar/4% H_2 was used as the sintering atmosphere in order to avoid the reduction of NiO to Ni, thus minimizing any possible high-temperature coarsening effect associated with metallic Ni. At the same time, compared with sintering in air, Ar was also expected not to facilitate the oxidation of SYT. The composition and preparation of various samples investigated in the present work is listed in Table 2.

2.2. Characterization

The crystal structure of SYT was determined by powder X-ray diffraction (XRD) with Cu K_α radiation (Siemens D5000).

Table 1
Explanation of the multi-component ceramic-based anode in this work

Component number	Material	Content (vol. %)	Properties	Roles
1	Y-substituted $SrTiO_3$	40–50	High electronic conductivity; negligible dimensional change upon redox cycling	Electronic conduction/current collection
2	YSZ	40–50	Considerable ionic conductivity; negligible dimensional change upon redox cycling	Ionic conduction
3	Ni	0–10	High catalytic activity for fuel oxidation	Catalyst

Table 2
List of samples prepared and characterized

Sample code	Composition (vol. %)	Method of Ni addition	Sintering conditions
ZrTi-1200	SYT:YSZ = 50:50	–	1200 °C in Ar/H_2
ZrTi5Ni-1200-IMP	SYT:YSZ:Ni = 47.5:47.5:5	Impregnation	1200 °C in Ar/H_2
ZrTi10Ni-1200-IMP	SYT:YSZ:Ni = 45:45:10	Impregnation	1200 °C in Ar/H_2
ZrTi5Ni-1300-IMP	SYT:YSZ:Ni = 47.5:47.5:5	Impregnation	1300 °C in Ar/H_2
ZrTi10Ni-1200-MIX	SYT:YSZ:Ni = 45:45:10	Mixing	1200 °C in Ar

The thermal and chemical expansion behavior of SYT and SYT/YSZ composite was measured using a push-rod dilatometer (Netzsch DIL 402C) with heating and cooling rates of 3 K min^{-1}. The dc four-probe method was used to measure the electrical conductivity of SYT and SYT/YSZ composite.

A three-electrode configuration schematically shown in Fig. 1 was adopted to characterize the electrochemical property of the anode. The active electrode area is 1 cm^2. Pt was used as the counter and reference electrodes. Gold mesh together with a small amount of gold paste was applied on top of the working electrode as current collector. Gold rings were used for sealing on both sides. The atmosphere at the working electrode was wet Ar/5% H_2 or wet H_2 (here "wet" means that the gas is saturated with water vapor at room temperature). Oxygen was used at the counter and reference electrodes. Electrochemical impedance spectroscopy (Impedance Spectrum Analyzer, IM6e, Zahner Meβtechnik) was used to measure the electrode polarization resistance under open circuit conditions. Selected samples were also measured under anodic polarization conditions. The observed open circuit voltages were in good agreement with the electromotive forces at various temperatures. Impedance spectra were recorded over a frequency range of 100 kHz–0.1 Hz with an ac amplitude of 10 mV. The gas flow rates were controlled at about 150 ml min^{-1}. The microstructure of the electrodes was investigated by scanning electron microscopy (SEM, LEO Gemini 1530 and a Zeiss Ultra55) and energy dispersive X-ray (EDX) analysis.

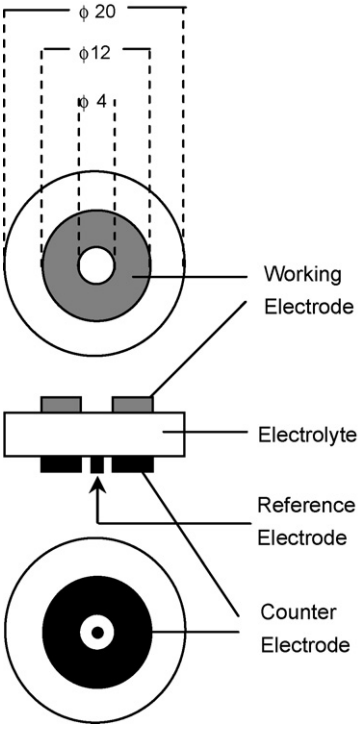

Fig. 1. The three-electrode cell configuration used in this work.

3. Results and discussion

3.1. Physical properties of the ceramic framework (SYT/YSZ)

The electrical conductivity of SYT depends to a very large extent on the preparation and processing procedures, i.e., the particular history of the sample [21]. Without applying a high-temperature (>1100 °C) reduction process, SYT does not show high electrical conductivity (>20 S cm^{-1}) under typical anode conditions. Similar behavior was observed with La-substituted $SrTiO_3$ (SLT) [10]. At a measurement temperature of 1000 °C, SLT samples sintered in Ar/H_2 at 1650 °C showed an electrical conductivity of 80–360 S cm^{-1}, while the conductivity of those sintered in air is only of order 1–16 S cm^{-1} under typical anode conditions. This behavior is considered to be related to the reduction/oxidation kinetics of transition of donor-substituted $SrTiO_3$ between a reduced state (good electronic conductor) and an oxidized state (poor electronic conductor) upon the variation of the oxygen partial pressure ($p(O_2)$) [23]. Although highly reduced SYT exhibited an initial conductivity of over 80 S cm^{-1}, it degraded upon redox cycling [21], indicating a new equilibrium state (with lower electrical conductivity than at the initial state) being approached. Nevertheless, it seems that a stable value in the order of 20–30 S cm^{-1} is attainable. Accordingly, the composite of SYT/YSZ (65/35 vol.%) displays a stable electrical conductivity of ∼10 S cm^{-1} under typical anode conditions, as shown in Fig. 2. It is still one order of magnitude lower than that of conventional Ni/YSZ cermet, but offers appreciable improvements over such materials as doped ceria or LSCM.

To test the reactivity of SYT with YSZ, a powder mixture with equal mass of SYT and YSZ was co-fired at 1400 °C for 5 h in Ar/4% H_2. According to the XRD results, no impurity phase was observed after co-firing, indicating good chemical compatibility between these two materials.

The thermal expansion coefficient of SYT is (11–12) × 10^{-6} K^{-1}, which is close to that of YSZ ((10.6–10.9) × 10^{-6} K^{-1} [24]). The chemical expansion of SYT at 830 °C between wet Ar/4% H_2 ($p(O_2) \sim 10^{-18}$ bar) and Ar/20% O_2 is 0.13–0.15%. The composite of SYT/YSZ (65/35 vol.%) displays even lower chemical expansion, i.e. 0.045% under the

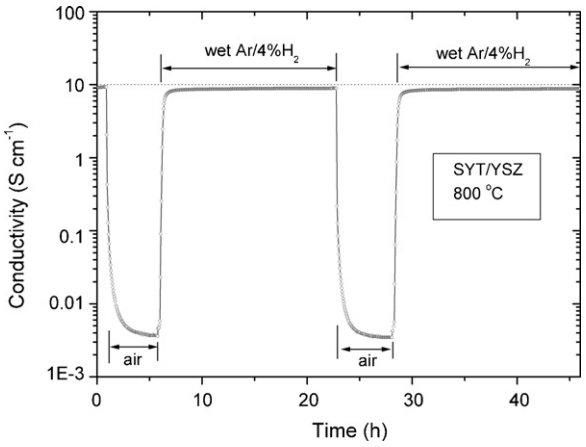

Fig. 2. Variation of electrical conductivity of a SYT/YSZ (65/35 vol.%) ceramic composite over two redox cycles between wet Ar/4% H_2 and air at 800 °C.

same experimental conditions, as shown in Fig. 3. As a reference, the chemical expansion of $Ce_{0.8}Gd_{0.2}O_{1.9-\delta}$ was also measured under the same experimental conditions and a value of ~0.17% was obtained. The chemical linear expansion of LSCM at 900 °C was 0.25–0.73% (0.8–2.2% volume expansion) between air and Ar/5% H_2 ($p(O_2) \sim 10^{-21}$ bar) [15]. It should be noted that $Ce_{0.8}Gd_{0.2}O_{1.9-\delta}$ and LSCM show lattice expanding on going from oxidizing to reducing conditions, opposite to SYT.

For an anode-supported planar SOFC, the expansion of the anode layer upon redox cycling will induce a tensile stress on the adjacent thin electrolyte layer. When the traditional Ni/YSZ cermet is used as the anode support, which is also called the anode current collector layer (ACCL), and an additional anode functional layer (AFL, with the same composition as ACCL but lower porosity than ACCL) is applied between the ACCL and the electrolyte layer, the expansion of ACCL/AFL upon redox cycling was found to be able to cause a strain of ~1% in the electrolyte layer, leading to electrolyte fracture [5]. Considering a typical anode/electrolyte bi-layer structure (500 μm thick anode and 8 μm thick YSZ electrolyte), and assuming the elastic modulus of the anode is 50–100 GPa, thermomechanical calculations using the general equations given in [25] indicate that the electrolyte is able to withstand a chemical expansion of 0.19–0.21% on the anode at 900 °C. In the calculation, mechanical parameters of the YSZ electrolyte at 900 °C were taken from the literature [26] (elastic modulus 155 GPa, flexural strength 265 MPa). Therefore, a strain of 0.045% observed with the SYT/YSZ composite in this study is likely to be low enough to avoid electrolyte fracture due to redox cycling.

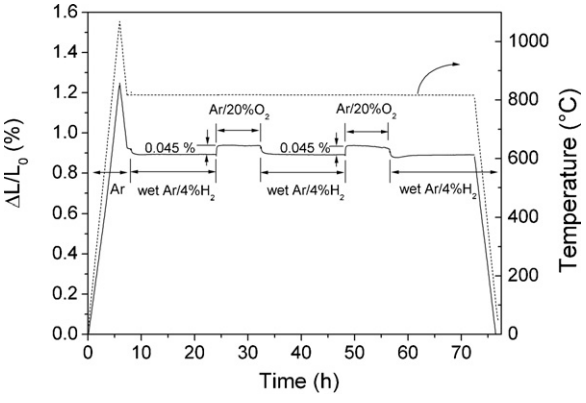

Fig. 3. Thermal and chemical expansion behaviors of SYT/YSZ (65/35 vol.%) ceramic composite. The sample was first heated up to 1060 °C and cooled down to 820 °C in Ar, then subjected to two redox cycles between wet Ar/4% H_2 and Ar/20% O_2 at 820 °C, and finally cooled down to room temperature.

3.2. Electrochemical performance and microstructures of SYT/YSZ/Ni anodes

Examples of impedance spectra obtained for different electrodes at various temperatures are given in Fig. 4. One or two arcs are generally observed. All impedance spectra were fitted to the equivalent circuit $LR_S(RQ)_1(RQ)_2$, following the circuit description codes defined elsewhere [27]. Here L is an inductance, R a resistance and Q a constant phase element. The inductance L is primarily ascribed to the leads, and a typical value is 10^{-6} H for the present measurement system. The series resistance, R_S, is mainly ascribed to the ohmic resistance of the electrolyte. Each (RQ) subcircuit describes a limiting process contributing an impedance arc. For spectra that seemed to contain only one distinct arc, attempts to fit them with only one (RQ) subcircuit often led to poor goodness of fit. Therefore, all the impedance

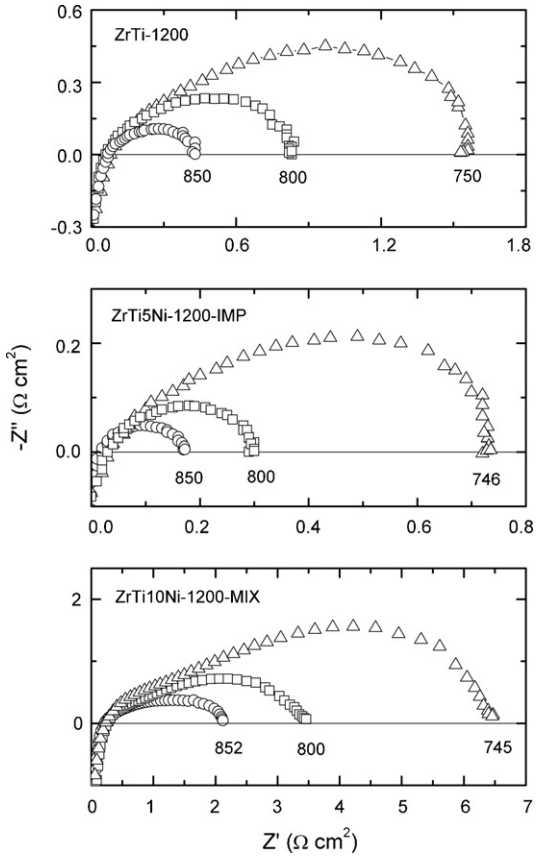

Fig. 4. Typical impedance spectra of the electrodes investigated in wet Ar/5% H_2 under open circuit conditions and at different temperatures. Numbers in the graph indicate the measurement temperatures in °C. The ohmic resistances were subtracted to compare only the polarization resistance.

data were fitted to the circuit $LR_S(RQ)_1(RQ)_2$. The polarization resistance of the electrode, R_p, is defined as $R_1 + R_2$. In many cases R_1 and R_2 cannot be determined separately with good certainty due to the overlap of these two arcs. However, the total polarization resistance R_p can be determined with a good certainty due to the well-defined low-frequency and high-frequency intercepts of the impedance spectra with the X-axis. In Fig. 4, ohmic resistances were subtracted from the impedance spectra to give only the polarization resistances for comparison. The as-obtained polarization resistances for all electrodes studied are plotted in Fig. 5 as a function of temperature.

One of these electrodes (ZrTi5Ni-1200-IMP) was tested in both wet Ar/5% H_2 and wet H_2. No significant change of the electrode performance was observed. It seems therefore that the electrode performance is not limited by the gas diffusion or hydrogen adsorption on the electrode surface under the present experimental conditions. Other samples were only measured in wet Ar/5% H_2.

The impedance spectra for selected samples were also measured under anodic polarization conditions. No clear dependence of the polarization resistance on the anode potential (E_a) (or discharging current) was observed. For instance, for the electrode ZrTi10Ni-1200-IMP at 750 °C (Fig. 6 a), the R_p at $E_a = -0.85$ V is slightly larger than that under open circuit conditions ($E_a = -1.020$ V). However, further increasing the anode potential leads to a decreased R_p. As a result, the R_p at $E_a = -0.700$ and -0.550 V is nearly the same as that under open circuit conditions. The electrode ZrTi5Ni-1200-IMP shows similar behavior (Fig. 6b). Thus it is considered that the polarization resistance measured under open circuit conditions is quite representative for the characterization of the electrochemical performance of the electrodes under study. The following discussions are therefore based on these values.

As expected, the electrode polarization resistance is significantly reduced with the addition of only a small amount of Ni by the impregnation method, demonstrating the catalytic role of the Ni particles. For instance, the R_p of 0%, 5% and 10% Ni-loaded

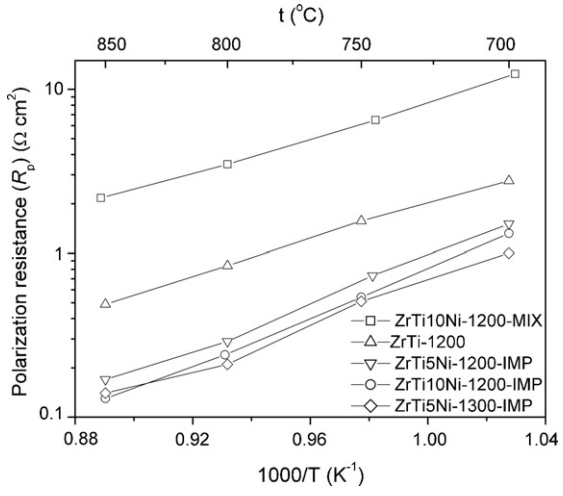

Fig. 5. Polarization resistances for all investigated electrodes listed in Table 2 as a function of temperature. All data were extracted from the impedance spectra obtained under open circuit conditions. The fuel gas is wet Ar/5% H_2.

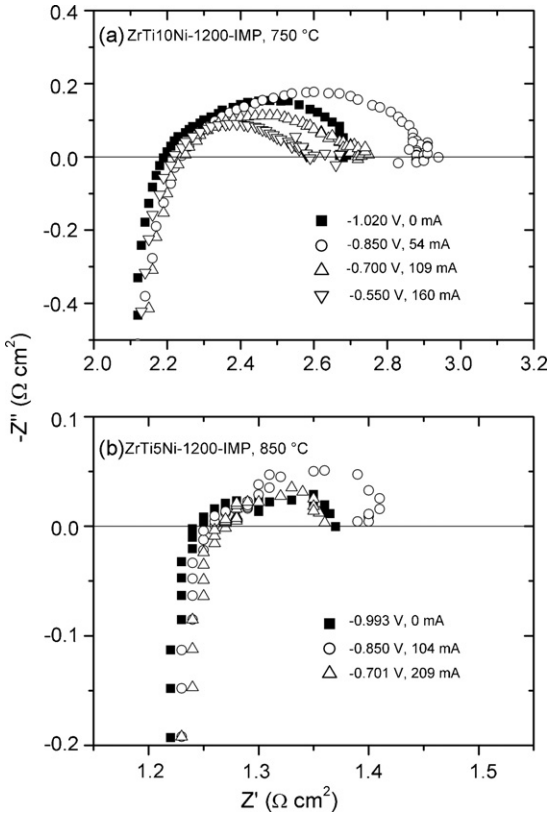

Fig. 6. Effect of anodic polarization on the impedance spectra of the electrodes investigated in wet Ar/5% H_2. The anode potential as well as the discharging current of the cell is indicated on the graph.

SYT/YSZ anodes (heat treated at 1200 °C for 3 h in Ar/4% H_2 before Ni-impregnation) in wet Ar/5% H_2 at 850 °C is 0.49, 0.17 and 0.13 Ω cm^2, respectively. Fig. 7 shows the microstructure of these electrodes. In the Ni-free electrode (Fig. 7a), the YSZ phase and SYT phase are well interlinked, with mean grain sizes of 0.3–0.5 μm and 1–2 μm, respectively. The larger grain size of the SYT phase could be caused by the high-temperature pre-reduction process. Fine and round Ni particles incorporated by the impregnation method can be easily identified in Fig. 7(b–d) due to their unique morphology. These are evenly dispersed onto the pore walls of the SYT/YSZ ceramic framework with particle sizes of 50–100 nm, offering a large number of active sites for the hydrogen oxidation reaction. In addition, they are not in contact with each other, and are thus not expected to suffer from grain coarsening. With large free pore volume around them, the dimensional change of Ni particles associated with redox cycling will have no detrimental effect on the integrity of the fuel cell.

Increasing the oxide electrodes sintering temperature from 1200 to 1300 °C offers further performance improvement. For instance, the R_p of a 5% Ni-loaded SYT/YSZ anode in wet Ar/5% H_2 at 800 °C is reduced from 0.29 to 0.21 Ω cm^2 when the sintering temperature is increased from 1200 to 1300 °C. This could be ascribed to better contacts between neighboring grains (i.e., SYT/SYT, YSZ/YSZ and SYT/YSZ) and better adhesion between the electrode and the electrolyte. The microstructure (Fig. 7d) shows an increased mean grain size of YSZ phase as the sintering temperature is increased. The grain size of SYT

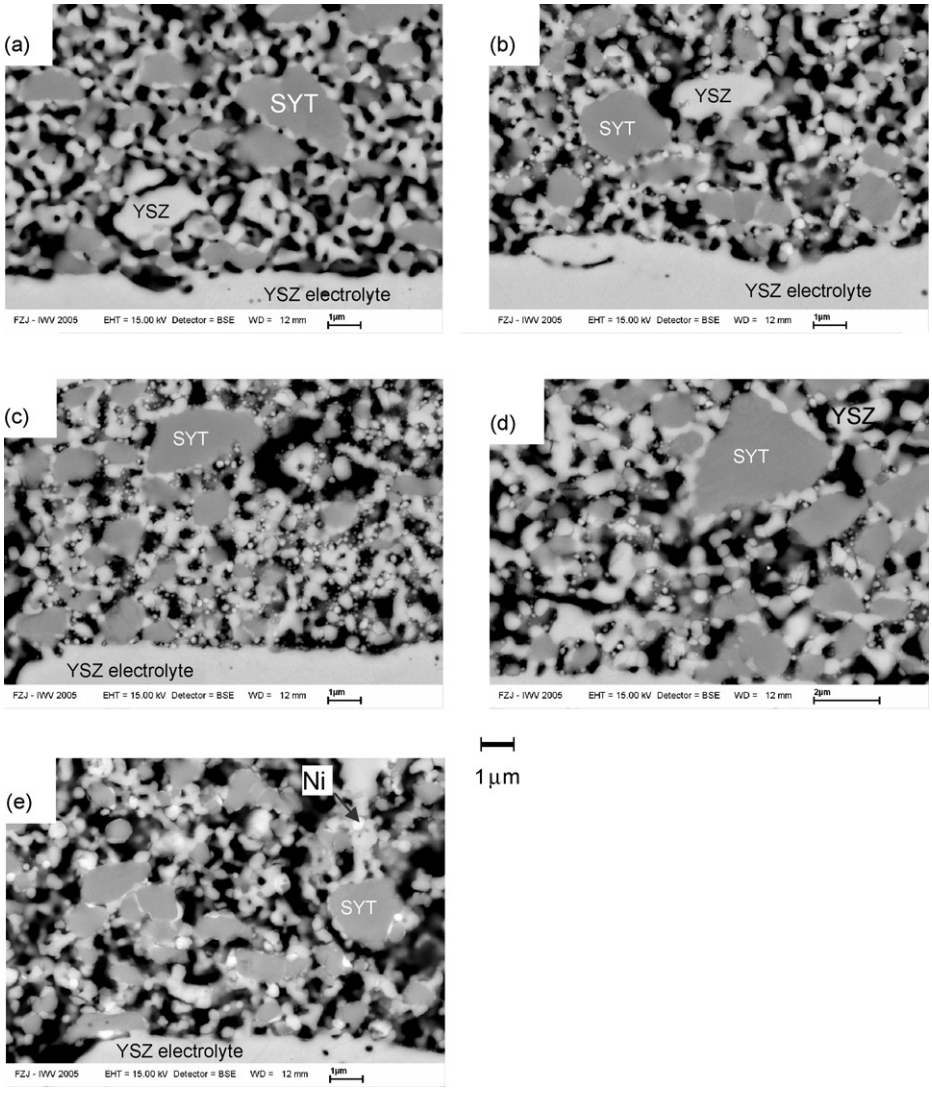

Fig. 7. SEM micrographs of the electrodes after electrochemical measurements. (a) ZrTi-1200; (b) ZrTi5Ni-1200-IMP; (c) ZrTi10Ni-1200-IMP; (d) ZrTi5Ni-1300-IMP; (e) ZrTi10Ni-1200-MIX. YSZ phase appears pale white, SYT phase grey and pores dark. Fine round Ni particles, attached to the pore walls, are visible in (b), (c) and (d) as compared with (a). They also appear slightly brighter than the YSZ phase. Ni particles in (e) are not so distinct from YSZ grains, but can be roughly distinguished according to their slightly greater brightness. One Ni particle is indicated by an arrow based on the EDX results.

phase does not change significantly since it has already been pre-reduced at 1300 °C for 12 h before being mixed with YSZ.

As a reference, a typical electrode polarization resistance (with gas conversion impedance [28] excluded) of a conventional Ni/YSZ cermet anode in wet H_2 is in the order of 0.05–0.1 $\Omega\,cm^2$ at 1000 °C, and 0.1–0.2 $\Omega\,cm^2$ at 850 °C [29,30]. Therefore, the electrochemical performance of the Ni-impregnated SYT/YSZ anodes studied in the present work is comparable with the conventional Ni/YSZ cermet anode.

Unusual results were observed, however, for the electrodes prepared by the mixing method. The R_p of the SYT/YSZ/Ni anode containing 10% Ni (ZrTi10Ni-1200-MIX) at 850 °C is as high as 2.2 $\Omega\,cm^2$, even higher than the Ni-free electrode (ZrTi-1200). The microstructure of this electrode is shown in Fig. 7e, where Ni particles can only be roughly distinguished according to their slightly higher brightness than YSZ grains. Certainly, the particle size of Ni particles in this electrode is much larger than those in the electrodes prepared by the impregnation method. Although nano-sized Ni particles were used as the starting material, they were possibly severely agglomerated during the sintering process. A larger Ni particle size will lead to a smaller catalytically active area. However, this explanation alone is not convincing, because the performance of this electrode is even poorer than the Ni-free electrode. It should be noted that Ar instead of Ar/4% H_2 was used as the protective atmosphere during the sintering of this electrode. The electronic conductivity is likely to be reduced significantly after this high-temperature process due to the relatively high $p(O_2)$ of Ar ($\sim 10^{-5}$ bar), as compared to Ar/4% H_2 ($\sim 10^{-15}$ bar at 1300 °C) in which the material was pre-reduced. Another possibility is that Ni reacts with SYT as with SLT [31], also leading to decreased electronic conductivity of SYT. However, EDX results on a number of large SYT grains gave no clear evidence of Ni in the ceramic phase. Thus, the impregnation method is

considered to be superior to the mixing method in that it avoids any high-temperature co-sintering process of Ni/NiO with other components in the electrode.

4. Conclusions

A new ceramic-based multi-component material was investigated in the search for alternative SOFC anode materials. This composite material consists of one electronic conductor (Y-substituted $SrTiO_3$, SYT), one ionic conductor (YSZ) and a small amount (∼5 vol.%) of Ni catalyst. The ceramic framework SYT/YSZ shows an electrical conductivity of $\sim 10\,S\,cm^{-1}$ under typical anode conditions. Despite the low content of Ni, this anode material exhibits very competitive electrochemical performance, as compared with the state-of-the-art Ni/YSZ cermet anode. For instance, a 5% Ni-impregnated SYT/YSZ anode shows a polarization resistance of $0.21\,\Omega\,cm^2$ at 800 °C in wet Ar/5%H_2. One of the most attractive features of this material is the good dimensional stability of the ceramic framework upon redox cycling. In this structure, volume changes of the Ni particles inside the pores of the ceramic framework will no longer cause any stress on the overall cell structure. Therefore an anode-supported planar SOFC using this anode material is expected to be redox-stable, which offers great advantages over the current generation of Ni/YSZ-based SOFCs. Further improvements can be achieved by, for example, the optimization of the electrode microstructure or the replacement of SYT/YSZ by other electronic/ionic conductors.

Acknowledgements

This research was supported by a Marie Curie International Fellowship (Q.X. Fu) under contract no MIF1-CT-2004-509999 within the 6th European Community Framework Programme. Part of this work was supported by the ESF (European Science Foundation) programme "Optimisation of Solid State Electrochemical Processes for Hydrocarbon Oxidation (OSSEP)". The authors thank P. Lersch (FZJ-IWV 2) for the XRD measurements and Dr. J. Malzbender (FZJ-IWV 2) for helpful discussions on the thermomechanical calculations.

References

[1] L.G.J. de Haart, K. Mayer, U. Stimming, I.C. Vinke, J. Power Sources 71 (1998) 302.
[2] G. Stathis, D. Simwonis, F. Tietz, A. Moropoulou, A. Naoumides, J. Mater. Res. 17 (2002) 951.
[3] T. Klemensø, C. Chung, P.H. Larsen, M. Mogensen, Solid oxide fuel cells IX, in: S.C. Singhal, J. Mizusaki (Eds.), The Electrochemical Society Proceedings Series, Pennington, NJ, 2005, p. 1226, PV 2005-07.
[4] D. Waldbillig, A. Wood, D.G. Ivey, Solid State Ionics 176 (2005) 847.
[5] J. Malzbender, E. Wessel, R.W. Steinbrech, Solid State Ionics 176 (2005) 2201.
[6] W. Halliop, A. Tuck, W.T. Thompson, Solid oxide fuel cells IX, in: S.C. Singhal, J. Mizusaki (Eds.), The Electrochemical Society Proceedings Series, Pennington, NJ, 2005, p. 191, PV 2005-07.
[7] G. Robert, A. Kaiser, E. Batawi, in: M. Mogensen (Ed.), Proceedings of the Sixth European Solid Oxide Fuel Cell Forum, European Fuel Cell Forum Oberrohrdorf Switzerland, 2004, p. 193.
[8] D. Waldbillig, A. Wood, D.G. Ivey, Solid oxide fuel cells IX, in: S.C. Singhal, J. Mizusaki (Eds.), The Electrochemical Society Proceedings Series, Pennington, NJ, 2005, p. 1245, PV 2005-07.
[9] P. Holtappels, J. Bradley, J.T.S. Irvine, A. Kaiser, M. Mogensen, J. Electrochem. Soc. 148 (8) (2001) A923.
[10] O.A. Marina, N.L. Canfield, J.W. Stevenson, Solid State Ionics 149 (2002) 21.
[11] J. Canales-Vázquez, S.W. Tao, J.T.S. Irvine, Solid State Ionics 159 (2003) 159.
[12] M. Mogensen, T. Lindegaard, U.R. Hansen, G. Mogensen, J. Electrochem. Soc. 141 (1994) 2122.
[13] O.A. Marina, C. Bagger, S. Primdahl, M. Mogensen, Solid State Ionics 123 (1999) 199.
[14] S.W. Tao, J.T.S. Irvine, Nat. Mater. 2 (2003) 320.
[15] S.W. Tao, J.T.S. Irvine, J. Electrochem. Soc. 151 (2) (2004) A252.
[16] S. Primdahl, Y.L. Liu, J. Electrochem. Soc. 149 (2002) A1466.
[17] H. Uchida, S. Suzuki, M. Watanabe, Electrochem. Solid-State Lett. 6 (2003) A174.
[18] J. Liu, B.D. Madsen, Z.Q. Ji, S.A. Barnett, Electrochem. Solid-State Lett. 5 (6) (2002) A122.
[19] N.Q. Minh, J. Am. Ceram. Soc. 76 (1993) 563.
[20] S.Q. Hui, A. Petric, J. Electrochem. Soc. 149 (1) (2002) J1.
[21] Q.X. Fu, F. Tietz, D. Stöver, Solid oxide fuel cells IX, in: S.C. Singhal, J. Mizusaki (Eds.), The Electrochemical Society Proceedings Series, Pennington, NJ, 2005, p. 1417, PV2005-07.
[22] M.P. Pechini, US Patent No. 3,330,697, July 11, 1967.
[23] U. Balachandran, N.G. Eror, J. Electrochem. Soc. 129 (1982) 1021.
[24] F. Tietz, G. Stochniol, A. Naoumidis, in: L.A.J.L. Sarton, H.B. Zeedijk (Eds.), Proceedings of the Fifth European Conference on Advanced Materials and Processes and Applications (Euromat '97), vol. 2, Netherlands Society for Materials Science, 1997, p. 271.
[25] C.-H. Hsueh, J. Appl. Phys. 91 (2002) 9652.
[26] A. Selçuk, A. Atkinson, J. Am. Ceram. Soc. 83 (2000) 2029.
[27] B.A. Boukamp, Solid State Ionics 169 (2004) 65.
[28] S. Primdahl, M. Mogensen, J. Electrochem. Soc. 145 (1998) 2431.
[29] S. Primdahl, M. Mogensen, J. Electrochem. Soc. 144 (1997) 3409.
[30] M. Brown, S. Primdahl, M. Mogensen, J. Electrochem. Soc. 147 (2000) 475.
[31] C. Pirovano, F. Tietz, unpublished results.